Molecular Dynamics Simulations of Polymer Welding: Strength from Interfacial Entanglements

Ting Ge,[1] Flint Pierce,[2,3] Dvora Perahia,[3] Gary S. Grest,[2] and Mark O. Robbins[1]
[1]Department of Physics and Astronomy, Johns Hopkins University, Baltimore, Maryland 21218, USA
[2]Sandia National Laboratories, Albuquerque, New Mexico 87185, USA
[3]Department of Chemistry, Clemson University, Clemson, South Carolina 29634, USA
(Received 20 November 2012; published 28 February 2013; corrected 6 March 2013)

Large-scale simulations of thermal welding of polymers are performed to investigate the rise of mechanical strength at the polymer-polymer interface with the welding time t_w. The welding process is at the core of integrating polymeric elements into devices as well as in the thermal induced healing of polymers, processes that require the development of interfacial strength equal to that of the bulk. Our simulations show that the interfacial strength saturates at the bulk shear strength long before polymers diffuse by their radius of gyration. Along with the strength increase, the dominant failure mode changes from chain pullout at the interface to chain scission as in the bulk. The formation of sufficient entanglements across the interface, which we track using a primitive path analysis, is required to arrest catastrophic chain pullout at the interface. The bulk response is not fully recovered until the density of entanglements at the interface reaches the bulk value. Moreover, the increase of interfacial strength before saturation is proportional to the number of interfacial entanglements between chains from opposite sides.

DOI: 10.1103/PhysRevLett.110.098301 PACS numbers: 82.35.Gh, 68.35.Fx, 81.20.Vj, 83.10.Mj

Thermal welding is a common means of joining polymeric elements [1,2]. Two polymer surfaces are brought into close contact above their glass transition temperature T_g and are allowed to interdiffuse for a welding time t_w. Polymer melt dynamics suggests that for homopolymer melts the properties of the weld should be indistinguishable from those of the bulk once the chains have diffused by about their radius of gyration R_g. In practice, however, welds reach the bulk strength at much shorter times [2]. A key question is what determines the rapid rise in interfacial strength and how it is related to mass uptake across the surface and polymer entanglement. Entanglements are topological constraints of polymers by other chains [3] that control their bulk viscoelastic and plastic responses.

Experiments have quantified the strength of welds by measuring the interfacial fracture toughness in tensile fracture and the peak shear strength of lap joints [4–6]. Both quantities grow as $t_w^{1/4}$ at short times and then saturate at their bulk values. Several different molecular mechanisms have been proposed to explain the scaling of strength with t_w. Some assume the strength is simply related to interpenetration depth [7–9] or the areal density of chain segments bridging the interface [10] or the contour length of bridging segments [11]. In many cases, these models are motivated by physical pictures of the development of entanglements at the interface, but chain friction may also be important [12].

It is difficult to distinguish between the proposed strengthening mechanisms with experiments. Entanglements are not directly observable, and experiments are usually restricted to the postanalysis of fracture surfaces [13] or bulk scattering [8], which does not isolate the response of the failing region. In contrast, computer simulations provide full spatial resolution throughout the failure process, allowing macroscopic stresses to be directly related to molecular structure and dynamics. Recently developed methods also enable the tracking of entanglements on a microscopic level [14–16].

In this Letter, we present results from large-scale molecular dynamics simulations of welding between surfaces of highly entangled homopolymers. The interfacial strength after a welding time t_w is determined by a simple shear test that mimics experiments [4–6]. As in the experiments, the interfacial strength rises linearly with $t_w^{1/4}$ before saturating at the bulk value well before the time t_d for the chains to diffuse a distance R_g. The dominant failure mechanism changes from chain pullout at small t_w to chain scission at large t_w and in the bulk. Evolution of entanglements during welding is tracked using a primitive path analysis algorithm [14,17]. The crossover to bulk response coincides with a rise in the entanglement density at the interface to the bulk density. Moreover, the areal density of entanglements between chains from opposing surfaces is linearly related to the interfacial strength at small t_w.

Our simulations employ a canonical bead-spring model [18] that captures the properties of linear homopolymers. Each polymer chain contains N spherical beads of mass m. All beads interact via the truncated, shifted Lennard-Jones (LJ) potential

$$U_{\mathrm{LJ}}(r) = 4u_0[(a/r)^{12} - (a/r)^6 - (a/r_c)^{12} + (a/r_c)^6], \quad (1)$$

where r_c is the cutoff radius and $U_{\mathrm{LJ}}(r) = 0$ for $r > r_c$. All quantities are expressed in terms of the molecular diameter a, the binding energy u_0, and the characteristic time $\tau = a(m/u_0)^{1/2}$.

For equilibration, beads along the chain were connected by an additional, unbreakable finitely extensible nonlinear elastic (FENE) potential

$$U_{\mathrm{FENE}}(r) = -\frac{1}{2}kR_0^2 \ln[1 - (r/R_0)^2], \quad (2)$$

with $R_0 = 1.5a$ and $k = 30u_0a^{-2}$. For mechanical tests, chain scission plays an essential role, and a simple quartic potential was used,

$$U_Q(r) = K(r - R_c)^2(r - R_c)(r - R_c - B) + U_0, \quad (3)$$

with $K = 2351u_0/k_B$, $B = -0.7425a$, $R_c = 1.5a$, and $U_0 = 92.74467u_0$. This potential gives the same equilibrium bond length as U_{FENE} and prevents chains from crossing each other so that entanglements can be studied. The bonds break at a force that is 100 times higher than that for breaking interchain bonds, consistent with experiments and previous simulations [19,20]. Previous work has shown that the entanglement length for this model is $N_e = 85 \pm 7$ and that the mechanical response for $N = 500$ is characteristic of highly entangled (large N) polymers [19,21–24].

The equations of motion were integrated using a velocity-Verlet algorithm with a time step $\delta t \leq 0.01\tau$. The temperature was held constant by a Langevin thermostat with a damping constant Γ [18]. A million τ will be abbreviated as $1M\tau$. All simulations were carried out using the LAMMPS parallel molecular dynamics code [25].

Two thin films were constructed following the standard methodology discussed by Auhl *et al.* [26]. Each film contains $M = 4800$ chains of length $N = 500$ beads or a total of 2.4 million beads. Periodic boundary conditions were applied along the x and y directions with dimensions $L_x = 700a$ and $L_y = 40a$. The thickness in the z direction was maintained at $L_z = 100a$ using two repulsive confining walls. Each film was well equilibrated at a temperature $T = 1.0u_0/k_B$ with $r_c = 2.5a$, $\Gamma = 0.1\tau^{-1}$, and pressure $P = 0$ maintained by expansion or contraction along the x direction. To form the welding interface at $z = 0$, the films were placed as close to contact as possible without overlap. The interdiffusion was along the z direction. During interdiffusion, volume was held fixed by repulsive walls perpendicular to the z direction.

After welding for a time t_w, the system was quenched rapidly below the glass temperature $T_g \approx 0.35u_0/k_B$. First, the cutoff radius was reduced to $r_c = 1.5a$ to decrease computational cost, reduce density changes, and facilitate comparison with past mechanical studies [19,21–24]. Then, the temperature was quenched at constant volume with a rate $\dot{T} = -10^{-3}u_0/(k_B\tau)$ to $T = 0.5u_0/k_B$, where $P = 0$. Subsequent quenching to $T = 0.2u_0/k_B$ was done at $\dot{T} = -2 \times 10^{-4}u_0/(k_B\tau)$ and $P = 0$. A Nose-Hoover barostat with time constant 50τ was applied to P_{xx} and P_{yy}. The repulsive walls were maintained at $z = \pm L_z$. We verified that our conclusions are not sensitive to the details of the quench protocol or geometry.

Shear was applied to the interface in a manner similar to a shear test of a lap joint [2]. Beads within $5a$ of the top and bottom were held rigid and displaced at constant velocity in opposite directions along the y axis. The average strain rate in the film $d\gamma/dt = 2 \times 10^{-4}\tau^{-1}$ was low enough that it did not affect the mode of failure, and stress had time to equilibrate across the system [27]. The shear stress σ was determined from the mean lateral force per unit area applied by the top and bottom walls. The temperature was maintained at $T = 0.2u_0/k_B$ with a Langevin thermostat ($\Gamma = 1\tau^{-1}$) acting only on the x component to avoid biasing the flow.

Stress-strain curves for polymer welds at different t_w are compared to the bulk response in Fig. 1(a). The bulk curve is typical of amorphous polymers. A narrow elastic region

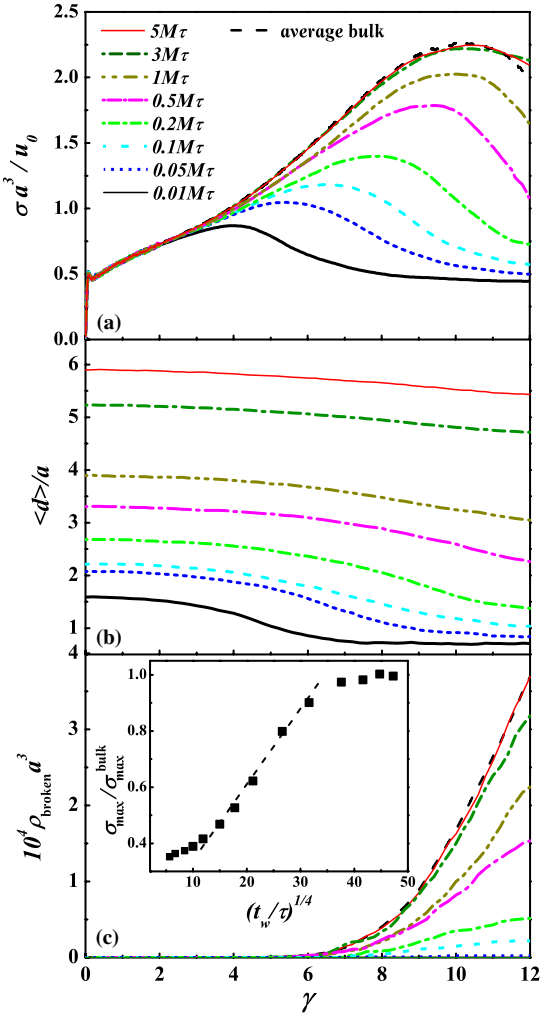

FIG. 1 (color online). (a) Shear stress σ versus shear strain γ for the indicated t_w. (b) Average interpenetration depth $\langle d \rangle$ versus strain. (c) Number density ρ_{broken} of broken bonds versus γ. The inset shows the maximum shear stress σ_{max} normalized by its average bulk value $\sigma_{\mathrm{max}}^{\mathrm{bulk}}$ versus $t_w^{1/4}$.

is followed by yield and strain hardening—a gradual increase in stress with strain. At sufficiently large strain, the material begins to fail. The shear stress reaches a maximum value $\sigma_{\max}^{\text{bulk}}$ and then drops.

Even for the shortest t_w, the stress-strain curve follows the bulk response up to $\gamma \sim 4$. As t_w increases, the stress follows the bulk curve to larger γ. For $t_w \geq 2M\tau$, the response is nearly indistinguishable from the bulk. In experiments, the strength of the weld is characterized by the maximum shear stress $\sigma_{\max}$ before failure and plotted against $t_w^{1/4}$ to test scaling predictions [2]. Our results, shown in the inset of Fig. 1(c), are very similar to experiments [2]. There is a constant strength from van der Waals (LJ) interactions at times too short for appreciable interdiffusion. The strength saturates to the bulk value as t_w increases past $1M\tau$ and is statistically indistinguishable from bulk behavior by about $3M\tau$. This is much shorter than the time for polymers to diffuse by their radius of gyration $t_d \gg 10M\tau$ [28]. At intermediate times, there is a linear rise in strength [dashed line, inset of Fig. 1(c)] that is consistent with $\sigma_{\max} \sim t_w^{1/4}$. Both simulations and experiments are limited to a factor of $\sim$3 change in stress that prevents a precise test of power law scaling. However, $t_w^{1/4}$ scaling is motivated by an assumption that strength is proportional to the interdiffusion distance. This is directly tested as described below.

Simulations allow the change in maximum stress to be correlated with changes in failure mechanism and molecular conformation. Strain leads to stretching and orientation of polymer chains that is directly related to strain hardening [23,29,30]. Starting near $\gamma \sim 4$, we see a noticeable tension along polymer backbones that grows rapidly with γ. This tension acts to pull back any chain segments that have diffused across the interface. One way to quantify chain pullout is to measure the evolution of the average interpenetration depth $\langle d \rangle$ of beads that have crossed the initial interface ($z = 0$) as a function of strain [Fig. 1(b)]. For $t_w < 0.1M\tau$, $\langle d \rangle$ begins to drop at the strain where the stress deviates from the bulk response and decreases most rapidly near $\sigma_{\max}$. The final interfacial width $\langle d \rangle$ is less than the size of a single bead and corresponds to complete chain pullout. At this point, the stress reaches a constant value that represents the friction between two separated films.

At larger t_w, chains cannot be pulled out from the opposing surface and the small ($\sim 0.5a$) decrease in $\langle d \rangle$ is consistent with conformational changes near chain ends in the bulk. The chains have diffused far enough that the tension required for chain pullout is high enough to break bonds along the backbone. Figure 1(c) shows the strain dependence of the number density ρ_{broken} of broken bonds averaged over the entire volume between moving layers. The curves for $t_w > 2M\tau$ are similar to the bulk. Bonds begin to break above $\gamma = 6$, and the highest rate of bond breaking is reached near $\gamma = 10$. This point coincides with the peak in shear stress that indicates mechanical failure. For $0.1M\tau < t_w < 2M\tau$, there is a crossover where the number of broken bonds rises rapidly and the amount of chain pullout measured by the drop in $\langle d \rangle$ decreases. At smaller t_w, bond breaking is localized near the initial interface. For $t_w > 2M\tau$, bonds break uniformly throughout the system, confirming that the interface has become as strong as the bulk. It is interesting to note that a similar transition from chain pullout to scission occurs with increasing chain length in previous simulations of craze formation [19,21,22]. Chain scission only occurs when chains are long enough to form entanglements (typically, $N > 2N_e$) that prevent chain pullout. By analogy, it is natural to expect that the transition to scission and bulk response occurs when chains have interdiffused enough to form entanglements at the interface.

Entanglements have proved elusive in experimental studies. However, the representation of entanglements as binary contacts between the primitive paths of polymer chains has provided many insights into the properties of polymer melts [14–16]. The primitive paths are obtained by fixing the chain ends and minimizing the chain length without allowing chain crossing. To limit excluded volume effects, the chain diameter is then decreased by a factor of 4 [17]. Contacts between the resulting primitive paths are counted to determine the number of topological constraints (TCs). We found that the ratio of the density of TCs, ρ_{TC}, to the bulk density, $\rho_{\text{TC}}^{\text{bulk}}$, was insensitive to the precise details of the procedure used to identify TCs. Past bulk studies show that ρ_{TC} is proportional to the entanglement density [14–17], and we refer to TCs and entanglements interchangeably below.

Figure 2(a) shows the normalized density of TCs as a function of height relative to the initial interface. At small t_w, the chains have not interdiffused enough to produce any entanglements at the interface, but there are two peaks near $z = \pm 10a$. These peaks reflect the fact that polymers near free surfaces are compressed perpendicular to the surface [31,32]. Chains in this pancakelike anisotropic conformation are subject to more TCs. As welding proceeds, diffusion increases the density of entanglements at the interface and reduces the peaks on either side. By $2.5M\tau$, the density has become nearly uniform across the system.

To correlate between $\sigma_{\max}$ and entanglements more quantitatively, we focus on the number of TCs between chains that are on opposite sides of the interface at $t_w = 0$. All of these are formed by interdiffusion, and it is natural that these interfacial entanglements should be most important in strengthening the interface by preventing chain pullout. Figure 2(b) shows the profiles of the normalized interfacial TC density ρ_{TC}^I. As the polymers diffuse, interfacial TCs spread outward from the interface and grow in number. The inset in Fig. 2(b) shows the correlation between the normalized weld strength $\sigma_{\max}/\sigma_{\max}^{\text{bulk}}$ and the areal density of interfacial TCs, N_{TC}^I/A. There is a linear

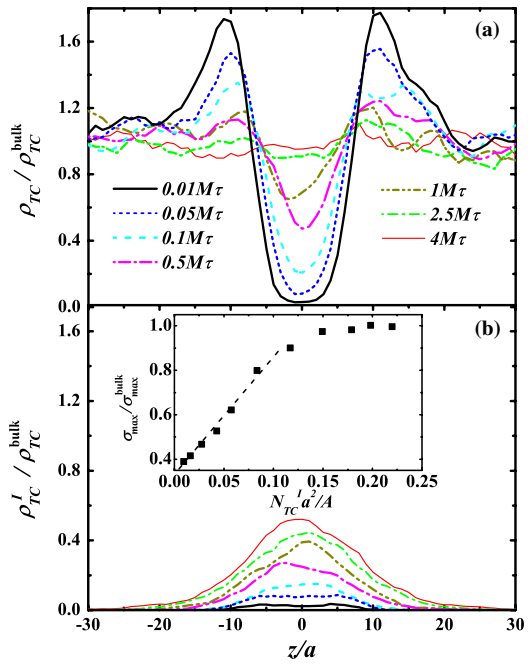

FIG. 2 (color online). Density profiles for (a) total and (b) interfacial TCs at the indicated t_w. The inset shows the reduced maximum shear stress versus the areal density of interfacial TCs N^I_{TC}/A. The error bars are comparable to the symbol size.

correlation between strength and interfacial entanglements at short times. At long times, the interfacial strength saturates while the number of interfacial entanglements continues to grow.

From the chain-packing model of entanglements [33–35], the number of interfacial entanglements N^I_{TC} scales with the volume spanned by chains that have diffused across the interface. This can be estimated as $2A\langle d\rangle$. Figure 3 confirms that there is a linear relation between N^I_{TC}/A and $\langle d\rangle$ over the entire range studied [36]. As noted above, welding models have generally assumed that $\sigma_{\max}$ rose linearly with $\langle d\rangle$ and then used reptation theory to argue that both scale as $t_w^{1/4}$. Subsequent work has shown

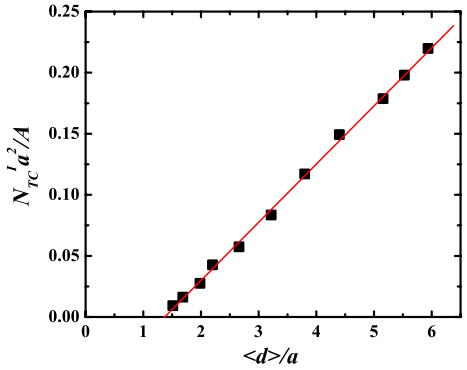

FIG. 3 (color online). The interfacial density of TCs N^I_{TC}/A versus the average interpenetration depth $\langle d\rangle$ and a linear fit.

that interfacial diffusion is more complicated because of the anisotropy that produces the peaks in entanglement density noted above and the prevalence of chain ends at the interface [2,28]. Indeed, recent simulations show that there is not a single simple scaling exponent over the range of times studied here [28]. Figures 2 and 3 show that, whatever the time dependence is, the fundamental factor determining strength is the entanglement density. One of the main differences between welding models is that some have assumed a simple proportionality between N^I_{TC}/A and $\langle d\rangle$ [2,7,10,12], while others assume a minimum interpenetration distance is needed for entanglements [9,37,38]. Figure 3 supports the latter interpretation, with a minimum distance $\sim 1.5a$ that is about one-third of the distance needed for saturation.

To summarize, we have demonstrated that the development of interfacial strength during welding is closely related to the formation of entanglements across the interface. The interface becomes mechanically indistinguishable from surrounding regions when the bulk entanglement density is recovered at the interface. There are then sufficient entanglements to prevent chain pullout at the interface, and the joint fails through the bulk mechanism of chain scission. Before the bulk strength is recovered, the interfacial strength rises linearly with the areal density of interfacial entanglements. This quantity is not accessible to experiments but is linearly related to the interdiffusion distance which has been measured.

These findings should help further development of theoretical descriptions of entanglement evolution across a polymer-polymer interface and constitutive molecular modeling of fracture in polymers. Of particular fundamental interest will be studies that vary the entanglement density by changing the entanglement length or making systems immiscible. An improved description of real experimental systems will require inclusion of chain polydispersity and the detailed process of crack propagation through lap shear joints [1,2]. Finally, studies at elevated temperatures could address the fracture of polymer melts where diffusion by the radius of gyration may be required to achieve bulk strength [39,40].

This work was supported in part by the National Science Foundation under Grants No. DMR-1006805, No. CMMI-0923018, No. OCI-0963185, and No. DMR-0907390. D. P. and G. S. G. acknowledge support from the U.S. Department of Energy Award No. DE-FG02-12ER46843. M. O. R. acknowledges support from the Simons Foundation. This research used resources at the National Energy Research Scientific Computing Center, which is supported by the Office of Science of the United States Department of Energy under Contract No. DE-AC02-05CH11231. Research was carried out in part at the Center for Integrated Nanotechnologies, a U.S. Department of Energy, Office of Basic Energy Sciences,

user facility. Sandia National Laboratories is a multiprogram laboratory managed and operated by Sandia Corporation, a wholly owned subsidiary of Lockheed Martin Corporation, for the U.S. Department of Energy's National Nuclear Security Administration under Contract No. DE-AC04-94AL85000.

[1] R. A. L. Jones and R. W. Richards, *Polymers at Surfaces and Interfaces* (Cambridge University Press, New York, 1999).
[2] R. P. Wool, *Polymer Interfaces: Structure and Strength* (Hanser, Munich, 1995).
[3] P. G. de Gennes, J. Chem. Phys. **55**, 572 (1971).
[4] K. Jud, H. H. Kausch, and J. G. Williams, J. Mater. Sci. **16**, 204 (1981).
[5] D. B. Kline and R. P. Wool, Polym. Eng. Sci. **28**, 52 (1988).
[6] R. Schnell, M. Stamm, and C. Creton, Macromolecules **31**, 2284 (1998).
[7] R. P. Wool and K. M. O'Connor, J. Appl. Phys. **52**, 5953 (1981).
[8] R. Schnell, M. Stamm, and C. Creton, Macromolecules **32**, 3420 (1999).
[9] H. R. Brown, Macromolecules **34**, 3720 (2001).
[10] S. Prager and M. Tirrell, J. Chem. Phys. **75**, 5194 (1981).
[11] P. G. de Gennes, C.R. Acad. Sci., Ser. 2 **308**, 1401 (1989).
[12] J. J. Benkoski, G. H. Fredrickson, and E. J. Kramer, J. Polym. Sci. B **40**, 2377 (2002).
[13] T. R. Russell, V. R. Deline, W. D. Dozier, G. P. Felcher, G. Agrawal, R. P. Wool, and J. W. Mays, Nature (London) **365**, 235 (1993).
[14] R. Everaers, S. K. Sukumaran, G. S. Grest, C. Svaneborg, A. Sivasubramanian, and K. Kremer, Science **303**, 823 (2004).
[15] M. Kröger, Comput. Phys. Commun. **168**, 209 (2005).
[16] C. Tzoumanekas and D. N. Theodorou, Macromolecules **39**, 4592 (2006).
[17] R. S. Hoy and G. S. Grest, Macromolecules **40**, 8389 (2007).
[18] K. Kremer and G. S. Grest, J. Chem. Phys. **92**, 5057 (1990).
[19] J. Rottler, S. Barsky, and M. O. Robbins, Phys. Rev. Lett. **89**, 148304 (2002).
[20] M. J. Stevens, Macromolecules **34**, 2710 (2001).
[21] J. Rottler and M. O. Robbins, Phys. Rev. Lett. **89**, 195501 (2002).
[22] J. Rottler and M. O. Robbins, Phys. Rev. E **68**, 011801 (2003).
[23] R. S. Hoy and M. O. Robbins, Phys. Rev. Lett. **99**, 117801 (2007).
[24] R. S. Hoy and M. O. Robbins, Phys. Rev. E **77**, 031801 (2008).
[25] S. Plimpton, J. Comp. Phys. **117**, 1 (1995).
[26] R. Auhl, R. Everaers, G. S. Grest, K. Kremer, and S. J. Plimpton, J. Chem. Phys. **119**, 12 718 (2003).
[27] J. Rottler and M. O. Robbins, Phys. Rev. E **68**, 011507 (2003).
[28] F. Pierce, D. Perahia, and G. S. Grest, Europhys. Lett. **95**, 46 001 (2011).
[29] T. Ge and M. O. Robbins, J. Polym. Sci. B **48**, 1473 (2010).
[30] K. Chen and K. S. Schweizer, Phys. Rev. Lett. **102**, 038301 (2009).
[31] D. N. Theodorou, Macromolecules **21**, 1400 (1988).
[32] A. Silberberg, J. Colloid Interface Sci. **125**, 14 (1988).
[33] Y.-H. Lin, Macromolecules **20**, 3080 (1987).
[34] L. J. Fetters, D. J. Lohse, D. Richter, T. A. Witten, and A. Zirkel, Macromolecules **27**, 4639 (1994).
[35] H. R. Brown and T. P. Russell, Macromolecules **29**, 798 (1996).
[36] To reduce the effects due to capillary waves at the interface, the width was measured from the local midplane, where the densities for beads from opposite sides are equal, rather than simply from $z = 0$.
[37] D. Adolf, M. Tirrell, and S. Prager, J. Polym. Sci., Polym. Phys. Ed. **23**, 413 (1985).
[38] A. G. Mikos and N. A. Peppas, J. Chem. Phys. **88**, 1337 (1988).
[39] R. Schach, Y. Tran, A. Menelle, and C. Creton, Macromolecules **40**, 6325 (2007).
[40] R. Schach and C. Creton, J. Rheol. **52**, 749 (2008).